International Journal of Innovative
Computing, Information and Control
Volume **12**, Number **2**, April **2016**

ICIC International ©2016 ISSN 1349-4198
pp. 651–663

FAULT TOLERANT ATTITUDE CONTROL FOR CUBESATS WITH INPUT SATURATION BASED ON DYNAMIC ADAPTIVE NEURAL NETWORK

Min Zhang, Xiaoning Shen and Tao Li

School of Information and Control
Nanjing University of Information Science and Technology
No. 219, Ningliu Road, Nanjing 210044, P. R. China
zhangmin@nuist.edu.cn; sxnystsyt@sina.com; litaojia@163.com

Received September 2015; revised December 2015

Abstract. *A fault-tolerant attitude control is presented to deal with uncertain external disturbances, small actuator faults and input saturation for cube satellites using 3-axis magnetorquers as attitude actuators in low earth orbit. The proposed control scheme achieves reconfigurable control capability by updating controller parameters adaptively according to the attitude state error. First, an H-infinity robust control with control hedging is designed for external distance and input saturation. Then, an adaptive dynamic neural network (NN) is adopted in the existing control loop to provide adaptive fault-tolerant control that can eliminate the influence of actuator faults. Due to accurate approximation of the dynamic NN and saturation supression of control hedging, control performance can be improved when actuator faults occur with input saturation. Numerical simulation for a double cube satellite was performed and the comparison results show that the proposed control method is effective.*

Keywords: Fault-tolerant control, Satellite attitude control, Input saturation, Robust control, Adaptive dynamic neural network

1. **Introduction.** Cube satellite (CubeSat) as a kind of small satellite which is generally in low earth orbit (LEO) and light enough to be feasible to use only 3-axis magnetorquers as actuators for attitude control gets more and more extensive attention due to its simple structure and modular design [1]. However, the attitude control for CubeSat investigated in theory is limited and almost not of enough capability to deal with some practical problems such as uncertain multiple external disturbances, input saturation, and actuator faults [2-5]. In fact, the working environment of CubeSat is not usually favourable, and various negative elements like those above-mentioned influence its normal operation [6]. So how to handle one of those problems or even all of them is obviously helpful for improving control performance during the period of satellite actual in-orbit operation. This article focuses on the practical in-orbit control issues in order to construct a fault tolerant control (FTC) law to keep the attitude stable whenever the satellite operates under desirable condition or under complex poor condition that there are external disturbance, or input saturation, or some actuation faults, or all of them. Note that, the article focuses on input saturation which gets little attention in current CubeSat study, but it usually exists at the time of operation beginning or actuator faults occurring. In order to avoid the negative influence on the attitude stability from input saturation in actual operation, the control approach for input saturation will be investigated in the article especially.

It is well known that attitude control is important in determining the location of satellites accurately and for reliable operation of satellites. Consequently, a significant amount of research has investigated attitude control based on several control approaches, such as

H-infinity robust control, feedback linearization and adaptive control [7-9], to address internal nonlinearity, uncertainties and external disturbances in a controlled system. However, most of these approaches cannot maintain satellite stability if actuators become faulty during attitude manoeuvres. Therefore, FTC capability must be addressed in the design of attitude control. FTC has been studied extensively [10]. Relative to the application of FTC to satellite attitude control, several studies have adopted various control theories, such as adaptive control, neural networks (NN), sliding mode control and fuzzy logic [11-13]. In addition, a study of satellite attitude tracking control with weak actuator faults examined the use of sliding mode control [14]. NNs have also been embedded into the control loop to achieve effective FTC [15]. A robust adaptive control method has been presented in [16] for attitude stabilization with external disturbance and actuator faults. Although most of these FTC methods can be used successfully for reaction wheel faults, the feasibility of such methods has not been proven for CubeSat attitude control systems in low earth orbit (LEO) using 3-axis magnetorquers as actuators. Consequently, designing an FTC scheme for CubeSat actuator faults, such as loss of magnetorquer effectiveness caused by deterioration of the coils used in 3-axis magnetic bars after a long working period, remains a challenge.

Another issue with attitude control of CubeSats with 3-axis magnetorquers in LEO is preventing factors, such as periodic changes in the geomagnetic field, gravitational torque, solar radiation, aerodynamic torque and internal noise, from negatively affecting the system [17]. Such factors result in nonlinearities and uncertainties in the system's mathematical model. H-infinity robust control has been extensively applied to systems with uncertain external disturbances because it can successfully maintain system states within the tolerant range by setting a desired bound norm value and, consequently, can maintain satisfactory attitude stability [18]. However, traditional H-infinity by itself is not an effective control for CubeSats; it does not handle nonlinearities from actuator faults and periodic changes in the geomagnetic field.

In this paper, a dynamic adaptive NN is embedded into the H-infinity robust control algorithm to provide adaptive FTC that triggers control reconfiguration when actuator faults occur, at the same time to deal with external disturbances and periodic changes in the geomagnetic field. The dynamic adaptive NN, which has good approximation accuracy, primarily reduces the influence of nonlinearities on system stability, which are caused by actuator faults and periodic changes in the geomagnetic field, while the H-infinity robust control suppresses the effects of external disturbances. The proposed adaptive FTC is an analytical redundancy-based system that can maintain stable CubeSat attitude. The proposed system can rearrange control effects when actuator faults occur [19].

Input saturation is also a critical problem in the application of FTC for CubeSats. In practice, magnetorquer output is constrained within a certain range or saturated due to the magnetorquer's physical mechanism. Therefore, control performance may deteriorate and become unstable if the actuator reaches saturation and fails to respond to control commands. To prevent input saturation from persisting for a long period, solutions for it in attitude control should be given sufficient consideration. According to various popular techniques for saturation in current literature [20-22], control hedging is an effective way and can be used conveniently to modify the existing H-infinity control algorithm to prevent the controlled system from control input saturation.

Therefore, this paper modifies the propesed adaptive FTC algorithm with control hedging in an attitude control system for CubeSats in LEO, and employed a double-unit (2U) CubeSat investigated in the well-known QB50 project [23] of Australian Center for Space Engineering Research to demonstrate the effectiveness of the presented FTC law. Here, H-infinity robust control with control hedging and an embedded dynamic adaptive NN in

the control loop are implemented to construct an adaptive FTC algorithm. The proposed method is intended to achieve effective control reconfiguration quickly and maintain attitude within a desired angle range by eliminating the negative effects of various factors, such as uncertain external disturbances, periodic changes in the geomagnetic field, control input saturation and sudden actuator faults.

The remainder of this paper is organized as follows. Section 2 summarizes the problem formulations. H-infinity robust control with control hedging is described in Section 3. In Section 4, the design of an adaptive FTC with a dynamic adaptive NN embedded in a closed-loop control system is described. Simulation results for a 2U CubeSat with the derived controller are given in Section 5. Finally, conclusions are presented in Section 6.

2. **Problem Formulations.** Consider a double CubeSat using magnetorquers in LEO. Nonlinear equations of attitude motion are given by the following kinematics and dynamics [24].

$$\begin{bmatrix} \dot{q}_0 \\ \dot{q}_1 \\ \dot{q}_2 \\ \dot{q}_3 \end{bmatrix} = \frac{1}{2} \begin{bmatrix} -q_1 & -q_2 & -q_3 \\ q_0 & -q_3 & q_2 \\ q_3 & q_0 & -q_1 \\ -q_2 & q_1 & q_0 \end{bmatrix} \begin{bmatrix} \omega_x \\ \omega_y \\ \omega_z \end{bmatrix} \tag{1}$$

$$\begin{bmatrix} \dot{\omega}_x \\ \dot{\omega}_y \\ \dot{\omega}_z \end{bmatrix} = \mathbf{I}_s^{-1} \begin{bmatrix} -\omega_y(\mathbf{I}_s\boldsymbol{\omega})_z + \omega_z(\mathbf{I}_s\boldsymbol{\omega})_y \\ \omega_x(\mathbf{I}_s\boldsymbol{\omega})_z - \omega_z(\mathbf{I}_s\boldsymbol{\omega})_x \\ -\omega_x(\mathbf{I}_s\boldsymbol{\omega})_y + \omega_y(\mathbf{I}_s\boldsymbol{\omega})_x \end{bmatrix} + \mathbf{I}_s^{-1}\mathbf{B}(t) \begin{bmatrix} T_x \\ T_y \\ T_z \end{bmatrix} + \mathbf{I}_s^{-1} \begin{bmatrix} w_{dx} \\ w_{dy} \\ w_{dz} \end{bmatrix} \tag{2}$$

Here, q_0, q_1, q_2, q_3 are the attitude quaternion variables, ω_x, ω_y, ω_z are the angle rates, the matrix $\mathbf{I}_s \in R^{3\times 3}$ includes the elements of the moment of inertia, $\mathbf{B}(t)$ is the local geomagnetic field matrix, T_x, T_y, T_z are magnetic dipole moments produced by a 3-axis magnetorquer, i.e., the control input elements, and w_{dx}, w_{dy}, w_{dz} are the external disturbances. $(\mathbf{I}_s\boldsymbol{\omega})_x$, $(\mathbf{I}_s\boldsymbol{\omega})_y$ and $(\mathbf{I}_s\boldsymbol{\omega})_z$ in Equation (2) are expressed as follows.

$$\begin{aligned} (\mathbf{I}_s\boldsymbol{\omega})_x &= I_{xx}\omega_x + I_{xy}\omega_y + I_{xz}\omega_z \\ (\mathbf{I}_s\boldsymbol{\omega})_y &= I_{yx}\omega_x + I_{yy}\omega_y + I_{yz}\omega_z \\ (\mathbf{I}_s\boldsymbol{\omega})_z &= I_{zx}\omega_x + I_{zy}\omega_y + I_{zz}\omega_z \end{aligned} \tag{3}$$

Suppose the system's equilibrium point is $\begin{bmatrix} q_0 & q_1 & q_2 & q_3 \end{bmatrix} = \begin{bmatrix} 1 & 0 & 0 & 0 \end{bmatrix}$. Thus, Equation (1) can be linearized around the equilibrium point, and the following equation is derived by further simplifying Equation (2):

$$\dot{\mathbf{x}}_1 = \begin{bmatrix} 0 \\ \frac{1}{2}\mathbf{I}_3 \end{bmatrix} \mathbf{x}_2 = \mathbf{T}\mathbf{x}_2 \tag{4}$$

$$\dot{\mathbf{x}}_2 = \mathbf{f}(\mathbf{x}_2) + \mathbf{I}_s^{-1}\mathbf{B}(t)\mathbf{u} + \mathbf{I}_s^{-1}\mathbf{w}_d \tag{5}$$

where $\mathbf{x}_1 = \begin{bmatrix} q_0 & q_1 & q_2 & q_3 \end{bmatrix}^T$, $\mathbf{x}_2 = \begin{bmatrix} \omega_x & \omega_y & \omega_z \end{bmatrix}^T$, $\mathbf{T} = \begin{bmatrix} 0 & \frac{1}{2}\mathbf{I}_3 \end{bmatrix}^T$, $\mathbf{I}_3$ is a unit matrix with 3 lines and 3 rows, $\mathbf{f}(\mathbf{x}_2) = \begin{bmatrix} -\omega_y(\mathbf{I}_s\boldsymbol{\omega})_z + \omega_z(\mathbf{I}_s\boldsymbol{\omega})_y \\ \omega_x(\mathbf{I}_s\boldsymbol{\omega})_z - \omega_z(\mathbf{I}_s\boldsymbol{\omega})_x \\ -\omega_x(\mathbf{I}_s\boldsymbol{\omega})_y + \omega_y(\mathbf{I}_s\boldsymbol{\omega})_x \end{bmatrix}$, $\mathbf{u} = \begin{bmatrix} T_x & T_y & T_z \end{bmatrix}^T$, and $\mathbf{w}_d = \begin{bmatrix} w_{dx} & w_{dy} & w_{dz} \end{bmatrix}^T$.

When each of the actuators partially loses its actuation effectiveness, Equations (4) and (5) can be rewritten as follows:

$$\begin{aligned} \dot{\mathbf{x}}(t) &= \begin{bmatrix} \mathbf{T}\mathbf{x}_2 \\ \mathbf{f}(\mathbf{x}_2, t) \end{bmatrix} + \begin{bmatrix} \mathbf{0} \\ \mathbf{I}_s^{-1}\mathbf{B}_0 \end{bmatrix} \mathbf{u}(t) + \begin{bmatrix} \mathbf{0} \\ \Delta\mathbf{f}(\mathbf{x}, \mathbf{u}, t) \end{bmatrix} + \begin{bmatrix} \mathbf{0} \\ \mathbf{I}_s^{-1}\mathbf{w}_d \end{bmatrix} \\ &= \mathbf{F}(\mathbf{x}(t), t) + \mathbf{B}\mathbf{I}_s^{-1}\mathbf{B}_0\mathbf{u}(t) + \mathbf{B}\Delta\mathbf{f}(\mathbf{x}(t), \mathbf{u}(t), t) + \mathbf{D}(t) \end{aligned} \tag{6}$$

where $\mathbf{x} = \begin{bmatrix} \mathbf{x}_1 & \mathbf{x}_2 \end{bmatrix}^T \in R^7$, $\mathbf{B} = \begin{bmatrix} 0 & \mathbf{I}_{3\times 3} \end{bmatrix}^T \in R^{7\times 3}$, $\mathbf{B}_0 \in R^{3\times 3}$ is the mean value of $\mathbf{B}(t)$, $\Delta\mathbf{f}(\mathbf{x},\mathbf{u},t) = \mathbf{I}_s^{-1}[\mathbf{B}(t) - \mathbf{B}_0]\mathbf{u}(t) + \Delta(\mathbf{x},\mathbf{u},t)$ is an uncertain nonlinear continuous function caused by actuator faults $\Delta(\mathbf{x},\mathbf{u},t)$ and local geomagnetic variation $\mathbf{I}_s^{-1}[\mathbf{B}(t) - \mathbf{B}_0]\mathbf{u}(t)$ and $\mathbf{D}(t) = \begin{bmatrix} 0 & \mathbf{I}_s^{-1}\mathbf{w}_d \end{bmatrix}^T$. If the attitude states are given as $\mathbf{x}_d = \begin{bmatrix} \mathbf{x}_{d1}^T & \mathbf{x}_{d2}^T \end{bmatrix}^T$, then the attitude error is defined as

$$\mathbf{e}(t) = \mathbf{x} - \mathbf{x}_d = \begin{bmatrix} \mathbf{x}_1 - \mathbf{x}_{d1} & \mathbf{x}_2 - \mathbf{x}_{d2} \end{bmatrix}^T = \begin{bmatrix} \mathbf{e}_1 & \mathbf{e}_2 \end{bmatrix}^T$$

Thus, the dynamic equation of the errors can be written as follows.

$$\dot{\mathbf{e}}(t) = \mathbf{F}(\mathbf{x}(t),t) + \mathbf{B}\mathbf{I}_s^{-1}\mathbf{B}_0\mathbf{u}(t) + \mathbf{B}\Delta\mathbf{f}(\mathbf{x}(t),\mathbf{u}(t),t) + \mathbf{D}(t) - \dot{\mathbf{x}}_d \tag{7}$$

Note that $\mathbf{I}_s^{-1}\mathbf{B}_0$ is invertible; therefore, the control law is given as follows:

$$\mathbf{u} = \left(\mathbf{I}_s^{-1}\mathbf{B}_0\right)^{-1}\left[\mathbf{u}_d + \mathbf{u}_n + \mathbf{B}^T\dot{\mathbf{x}}_d - \mathbf{f}(\mathbf{x}_2,t)\right] \tag{8}$$

where $\mathbf{u}_d = \mathbf{K}\mathbf{e}$ is the output of robust control and $\mathbf{u}_n$ is the output of the dynamic adaptive NN. Equation (8) is substituted into Equation (7) to obtain the following.

$$\begin{aligned}
\dot{\mathbf{e}}(t) &= \mathbf{F}(\mathbf{x}(t),t) + \mathbf{B}\Delta\mathbf{f}(\mathbf{x}(t),\mathbf{u}(t),t) + \mathbf{D}(t) - \dot{\mathbf{x}}_d + \mathbf{B}\mathbf{K}\mathbf{e}(t) \\
&\quad + \mathbf{B}\mathbf{u}_n + \mathbf{B}\mathbf{B}^{\mathbf{T}}\dot{\mathbf{x}}_d - \mathbf{B}\mathbf{f}(\mathbf{x}_2,t) \\
&= \left[\mathbf{F}(\mathbf{x}(t),t) - \dot{\mathbf{x}}_d + \mathbf{B}\mathbf{B}^{\mathbf{T}}\dot{\mathbf{x}}_d - \mathbf{B}\mathbf{f}(\mathbf{x}_2,t)\right] + \mathbf{B}\mathbf{K}\mathbf{e}(t) + \mathbf{D}(t) \\
&\quad + \mathbf{B}\mathbf{u}_n + \mathbf{B}\Delta\mathbf{f}\left(\mathbf{x}(t),\mathbf{u}(t),t\right) \\
&= \begin{bmatrix} \mathbf{T}\mathbf{x}_2 \\ \mathbf{f}(\mathbf{x}_2,t) \end{bmatrix} - \begin{bmatrix} \mathbf{0} \\ \mathbf{f}(\mathbf{x}_2,t) \end{bmatrix} - \begin{bmatrix} \dot{\mathbf{x}}_{1d} \\ \dot{\mathbf{x}}_{2d} \end{bmatrix} + \begin{bmatrix} \mathbf{0} \\ \dot{\mathbf{x}}_{2d} \end{bmatrix} + \mathbf{B}\mathbf{K}\mathbf{e}(t) + \mathbf{D}(t) \\
&\quad + \mathbf{B}\mathbf{u}_n + \mathbf{B}\Delta\mathbf{f}(\mathbf{x}(t),\mathbf{u}(t),t) \\
&= \begin{bmatrix} \mathbf{T}\mathbf{x}_2 \\ \mathbf{0} \end{bmatrix} - \begin{bmatrix} \dot{\mathbf{x}}_{1d} \\ \mathbf{0} \end{bmatrix} + \mathbf{B}\mathbf{K}\mathbf{e}(t) + \mathbf{D}(t) + \mathbf{B}\mathbf{u}_n + \mathbf{B}\Delta\mathbf{f}(\mathbf{x}(t),\mathbf{u}(t),t) \\
&= \begin{bmatrix} \mathbf{T}\mathbf{e}_2 \\ \mathbf{0} \end{bmatrix} + \mathbf{B}\mathbf{K}\mathbf{e}(t) + \mathbf{D}(t) + \mathbf{B}\mathbf{u}_n + \mathbf{B}\Delta\mathbf{f}(\mathbf{x}(t),\mathbf{u}(t),t) \\
&= (\mathbf{A} + \mathbf{B}\mathbf{K})\mathbf{e}(t) + \mathbf{D}(t) + \mathbf{B}\mathbf{u}_n + \mathbf{B}\Delta\mathbf{f}(\mathbf{x}(t),\mathbf{u}(t),t)
\end{aligned} \tag{9}$$

Here, $\mathbf{A} = \begin{bmatrix} \mathbf{0} & \mathbf{T} \\ \mathbf{0} & \mathbf{0} \end{bmatrix} \in R^{7\times 7}$. Equation (9) shows that the system can achieve closed-loop stability by carefully choosing $\mathbf{u}_n$ to eliminate the impact of $\Delta\mathbf{f}(\mathbf{x}(t),\mathbf{u}(t),t)$, and choosing appropriate $\mathbf{K}$ in the H-infinity robust control algorithm to eliminate disturbance element $\mathbf{D}(t)$.

3. **H-Infinity Robust Control with Control Hedging.** Based on Equation (9), the H-infinity robust control algorithm is first investigated here for a desired error dynamics equation that is free from $\Delta\mathbf{f}(\mathbf{x}(t),\mathbf{u}(t),t)$. So in this section, we prior assume $\Delta\mathbf{f}(\mathbf{x}(t),\mathbf{u}(t),t) = 0$ and $\mathbf{u}_n = 0$, and then deduce the H-infinity robust control algorithm with control hedging mainly for disturbance item $\mathbf{D}(t)$ and input saturation in the following equation:

$$\dot{\mathbf{e}}(t) = (\mathbf{A} + \mathbf{B}\mathbf{K})\mathbf{e}(t) + \mathbf{D}(t) \tag{10}$$

The control input saturation function is defined as follows:

$$\delta_i = g(u_i) = \begin{cases} u_i, & |u_i| \le \delta_{0i} \\ \delta_{0i}\dfrac{u_i}{|u_i|}, & |u_i| > \delta_{0i} \end{cases}, \quad i = 1,2,3 \tag{11}$$

where δ_{0i} is the maximum value of the ith axis actuator and $\boldsymbol{\delta} = [\delta_1,\delta_2,\delta_3]$ is the input saturation vector.

Accordingly, the control hedging is designed as follows.

$$\mathbf{u}_h = \boldsymbol{\delta} - \mathbf{u}_n \tag{12}$$

The robust control law with control hedging is obtained as follows by inserting Equation (12) into primary robust control $\mathbf{u}_d$ to prevent the system from being influenced by actuator saturation.

$$\mathbf{u}_{dh} = \mathbf{u}_d - \mathbf{u}_h = \mathbf{K}\mathbf{e} - \mathbf{u}_h \tag{13}$$

The following content discusses stability of the system controlled by H-infinity robust control with control hedging. The H-infinity performance index is set as follows.

$$\int_0^\infty \mathbf{e}^T(t)\mathbf{Q}\mathbf{e}(t)dt \le \mathbf{e}^T(0)\mathbf{P}\mathbf{e}(0) + \gamma^2 \int_0^\infty \mathbf{D}^T(t)\mathbf{D}(t)dt \tag{14}$$

Here, γ is a given positive value, $\mathbf{Q}$ is a given positive definite symmetric constant matrix, and $\mathbf{P}$ is a positive definite symmetric constant matrix to be calculated.

Theorem 3.1. *Given $\gamma > 0$, $\mathbf{Q} = \mathbf{Q}^T > 0$ such that the following Riccati equation has a solution for the positive definite symmetric matrix $\mathbf{P}$,*

$$\mathbf{A}^T\mathbf{P} + \mathbf{P}\mathbf{A} - \mathbf{P}\left(2\mathbf{B}\mathbf{B}^T\mathbf{Q}^{-1}\mathbf{B}\mathbf{B}^T - \frac{1}{\gamma^2}\mathbf{I}\right)\mathbf{P} + \mathbf{Q} + \mathbf{I} = 0 \tag{15}$$

The closed-loop gain is

$$\mathbf{K} = -\mathbf{B}^T\mathbf{Q}^{-1}\mathbf{B}\mathbf{B}^T\mathbf{P} \tag{16}$$

Then, system (10) is of bounded closed-loop stability with the H-infinity norm bound γ and satisfies the performance index (14).

Proof: Consider the following Lyapunov candidate function $V(x) = \mathbf{e}^T(t)\mathbf{P}\mathbf{e}(t)$. Suppose $\mathbf{D}(t) = 0$. We can then obtain $\dot{V}(x) = \mathbf{e}^T(t)[(\mathbf{A}+\mathbf{B}\mathbf{K})^T\mathbf{P} + \mathbf{P}(\mathbf{A}+\mathbf{B}\mathbf{K})]\mathbf{e}(t)$. In view of Equations (15) and (16), the following inequality can be derived.

$$\dot{V}(x) = \mathbf{e}^T(t)\left[\mathbf{A}^T\mathbf{P} + \mathbf{P}\mathbf{A} - 2\mathbf{P}\mathbf{B}^T\mathbf{Q}^{-1}\mathbf{B}\mathbf{B}^T\mathbf{P}\right]\mathbf{e}(t) < 0$$

Thus, the closed-loop system $\dot{\mathbf{e}}(t) = (\mathbf{A}+\mathbf{B}\mathbf{K})\mathbf{e}(t)$ is asymptotically stable.

Note that $\mathbf{A}_d = \mathbf{A} + \mathbf{B}\mathbf{K}$. Here, we discuss the robust stability of the closed-loop system (10). First, we obtain the following expression based on the expansion of the left equation in Equation (14).

$$\begin{aligned}\int_0^\infty \mathbf{e}^T(t)\mathbf{Q}\mathbf{e}(t)dt =& \mathbf{e}^T(0)\mathbf{P}\mathbf{e}(0) - \mathbf{e}^T(\infty)\mathbf{P}\mathbf{e}(\infty) \\ &+ \int_0^\infty \left\{\mathbf{e}^T(t)\mathbf{Q}\mathbf{e}(t) + \frac{d}{dt}\left[\mathbf{e}^T(t)\mathbf{P}\mathbf{e}(t)\right]\right\}dt\end{aligned}$$

As $\mathbf{e}^T(\infty)\mathbf{P}\mathbf{e}(\infty) \ge 0$ and Equations (10), (13) and (16) are substituted into the above expression, we obtain the following.

$$\begin{aligned}&\int_0^\infty \mathbf{e}^T(t)\mathbf{Q}\mathbf{e}(t)dt \\ &\le \mathbf{e}^T(0)\mathbf{P}\mathbf{e}(0) + \int_0^\infty \left\{\mathbf{e}^T(t)\mathbf{Q}\mathbf{e}(t) + \frac{d}{dt}\left[\mathbf{e}^T(t)\mathbf{P}\mathbf{e}(t)\right]\right\}dt \\ &= \mathbf{e}^T(0)\mathbf{P}\mathbf{e}(0) + \int_0^\infty \left\{\mathbf{e}^T(t)\mathbf{Q}\mathbf{e}(t) + \mathbf{e}^T(t)\left[\mathbf{P}\mathbf{A}_d + \mathbf{A}_d^T\mathbf{P}\right]\mathbf{e}(t) + \mathbf{e}^T(t)\mathbf{P}\mathbf{D}(t)\right. \\ &\quad \left. + \mathbf{D}^T(t)\mathbf{P}\mathbf{e}(t) - \gamma^2\mathbf{D}^T(t)\mathbf{D}(t) + \gamma^2\mathbf{D}^T(t)\mathbf{D}(t) - \frac{1}{\gamma^2}\mathbf{e}^T(t)\mathbf{P}\mathbf{P}\mathbf{D}(t) + \frac{1}{\gamma^2}\mathbf{e}^T(t)\mathbf{P}\mathbf{P}\mathbf{D}(t)\right.\end{aligned}$$

$$
\begin{aligned}
&-\mathbf{u}_h^T\mathbf{B}^T\mathbf{P}\mathbf{e}(t)-\mathbf{e}^T\mathbf{P}\mathbf{B}\mathbf{u}_h\Big\}dt \\
&=\mathbf{e}^T(0)\mathbf{P}\mathbf{e}(0)+\int_0^\infty\Big\{\mathbf{e}^T(t)\mathbf{Q}\mathbf{e}(t)+\mathbf{e}^T(t)\left[\mathbf{P}\mathbf{A}_d+\mathbf{A}_d^T\mathbf{P}\right]\mathbf{e}(t)-\left[\frac{1}{\gamma}\mathbf{P}\mathbf{e}(t)-\gamma\mathbf{D}(t)\right]^T \\
&\quad\bullet\left[\frac{1}{\gamma}\mathbf{P}\mathbf{e}(t)-\gamma\mathbf{D}(t)\right]+\gamma^2\mathbf{D}^T(t)\mathbf{D}(t)+\frac{1}{\gamma^2}\mathbf{e}^T(t)\mathbf{P}\mathbf{P}\mathbf{e}(t)-\mathbf{u}_h^T\mathbf{B}^T\mathbf{P}\mathbf{e}(t)-\mathbf{e}^T\mathbf{P}\mathbf{B}\mathbf{u}_h\Big\}dt \\
&\le\mathbf{e}^T(0)\mathbf{P}\mathbf{e}(0)+\int_0^\infty\mathbf{e}^T(t)\left[\mathbf{Q}+\mathbf{P}\mathbf{A}_d+\mathbf{A}_d^T\mathbf{P}+\frac{1}{\gamma^2}\mathbf{P}\mathbf{P}\right]\mathbf{e}(t)dt+\int_0^\infty\gamma^2\mathbf{D}^T(t)\mathbf{D}(t)dt \\
&\quad+2\int_0^\infty\|\mathbf{e}(t)\|\,\|\mathbf{P}\mathbf{B}\|\,\|\mathbf{u}_h\|\,dt
\end{aligned}
$$

Here, let $\mathbf{M}=\mathbf{A}_d^T\mathbf{P}+\mathbf{P}\mathbf{A}_d+\frac{1}{\gamma^2}\mathbf{P}\mathbf{P}+\mathbf{Q}$. From Equations (15) and (16), the inequality can be derived as follows.

$$\mathbf{M}=\mathbf{A}_d^T\mathbf{P}+\mathbf{P}\mathbf{A}_d+\frac{1}{\gamma^2}\mathbf{P}\mathbf{P}+\mathbf{Q}=\mathbf{A}^T\mathbf{P}+\mathbf{P}\mathbf{A}-2\mathbf{P}\mathbf{B}\mathbf{B}^T\mathbf{Q}^{-1}\mathbf{B}\mathbf{B}^T\mathbf{P}+\frac{1}{\gamma^2}\mathbf{P}\mathbf{P}+\mathbf{Q}<0$$

The minimum eigenvalue of $\mathbf{M}$ is $\lambda=\lambda_{\min}(\mathbf{M})$. Based on Equation (11), it is obvious that $\|\boldsymbol{\delta}\|\le\delta_0$. Note that the $\mathbf{u}_n$ is normally designed to be bounded. Therefore, both control input $\mathbf{u}_n$ and saturation input $\boldsymbol{\delta}$ are bounded. Then, the inequality can be obtained when $\|\mathbf{e}(t)\|\ge\frac{\|\mathbf{P}\mathbf{B}\|(\|\mathbf{u}_n\|+\|\boldsymbol{\delta}\|)}{\lambda}$.

$$\int_0^\infty\mathbf{e}^T(t)\mathbf{M}\mathbf{e}(t)dt+2\int_0^\infty\|\mathbf{e}(t)\|\,\|\mathbf{P}\mathbf{B}\|\,\|\mathbf{u}_h\|dt<0$$

Thus, the following inequality can be satisfied.

$$\int_0^\infty\mathbf{e}^T(t)\mathbf{Q}\mathbf{e}(t)dt\le\mathbf{e}^T(0)\mathbf{P}\mathbf{e}(0)+\int_0^\infty\gamma^2\mathbf{D}^T(t)\mathbf{D}(t)\}dt$$

This also means the performance index (13) is satisfied, which completes the proof.

4. **Adaptive FTC by Embedding Dynamic Adaptive NN into Closed-Loop Control.** In this section, we will construct a kind of adaptive FTC by designing $\mathbf{u}_n$ embedded into the robust control (13) in order to eliminate the influence of $\Delta\mathbf{f}(\mathbf{x}(t),\mathbf{u}(t),t)$ that is composed of some actuator faults and local periodic geomagnetic variation. The whole control system schematic diagram is illustrated in Figure 1.

A type of dynamic adaptive NN is designed to compensate for the influence of the uncertain nonlinear function $\Delta\mathbf{f}(\mathbf{x},\mathbf{u},t)$ in Equation (9). The output of the dynamic adaptive NN is designed as follows:

$$\mathbf{u}_n=\mathbf{u}_{nn}+\mathbf{u}_{ns} \tag{17}$$

where $\mathbf{u}_{nn}$ is the output of the NN, and $\mathbf{u}_{ns}$ is its compensation for the approximation error. By modifying the fully tuned adaptive radial basis function NN (RBF NN) [25] and a dynamic structure NN [26], a type of dynamic adaptive RBF NN with variable topological structure and on-line updating of network parameters is presented to achieve $\mathbf{u}_n$ with excellent accurate approximation performance. The following equation can be obtained because the dynamic adaptive RBF NN has the same approximation property as a fully tuned RBF NN.

$$\Delta\mathbf{f}(\mathbf{x},\mathbf{u},t)=\mathbf{W}^{*T}\mathbf{G}^*(\mathbf{X},\boldsymbol{\xi}^*,\boldsymbol{\eta}^*)+\boldsymbol{\varepsilon}(\mathbf{X}) \tag{18}$$

Here, $\mathbf{X}=[\mathbf{x}^T,\mathbf{e}^T,t]^T\in R^{11}$ is the input vector of the dynamic adaptive RBF NN and $\mathbf{X}\in\mathbf{N}_d$. Note that $\mathbf{N}_d$ is a sufficiently large compact set. $\mathbf{W}^*$, $\boldsymbol{\xi}^*$ and $\boldsymbol{\eta}^*$ denote the ideal constant weight, centre and width, respectively, and $\boldsymbol{\varepsilon}(\mathbf{X})$ is the approximation error that

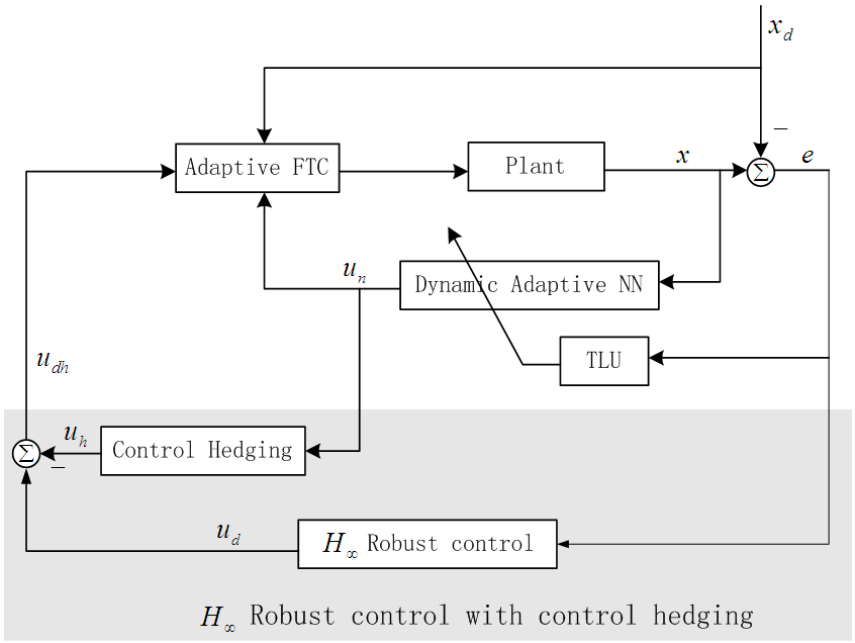

FIGURE 1. Control system schematic diagram

satisfies $\boldsymbol{\varepsilon}_I = \sup_{\mathbf{X}_i \in \mathbf{N}_d} \|\boldsymbol{\varepsilon}(\mathbf{X})\|$. $\mathbf{G}^*$ denotes the ideal vector function composed of commonly used Gaussian functions. The output $\mathbf{u}_{nn}$ of the dynamic adaptive RBF NN is defined as follows.

$$\mathbf{u}_{nn} = -\hat{\mathbf{W}}^T \hat{\mathbf{G}} \left(\mathbf{X}, \hat{\boldsymbol{\xi}}, \hat{\boldsymbol{\eta}} \right) \tag{19}$$

where, $\hat{\mathbf{W}}$, $\hat{\boldsymbol{\xi}}$ and $\hat{\boldsymbol{\eta}}$ are estimations. The Taylor's series of $\mathbf{G}^* \left(\mathbf{X}, \boldsymbol{\xi}^*, \boldsymbol{\eta}^* \right)$ is taken at $\boldsymbol{\xi}^* = \hat{\boldsymbol{\xi}}$ and $\boldsymbol{\eta}^* = \hat{\boldsymbol{\eta}}$. Then, by substituting Equations (17) and (18) into Equation (9), we obtain the following equation after simplification. Note that according to Theorem 3.1, the external disturbances will not be considered here for the feedback matrix $\mathbf{K}$ can eliminate its negative; thus, $\mathbf{D}(t) = 0$ is assumed.

$$\dot{\mathbf{e}}(t) = (\mathbf{A} + \mathbf{BK})\mathbf{e}(t) + \mathbf{B}\tilde{\mathbf{W}}^T \hat{\mathbf{G}} + \mathbf{B}\hat{\mathbf{W}}^T \left(\hat{\mathbf{G}}'_\xi \tilde{\boldsymbol{\xi}} + \hat{\mathbf{G}}'_\eta \tilde{\boldsymbol{\eta}} \right) + \mathbf{BE} - \mathbf{B}\mathbf{u}_{ns} \tag{20}$$

Here, $\tilde{\mathbf{W}} = \mathbf{W}^* - \hat{\mathbf{W}}$, $\tilde{\mathbf{G}} = \mathbf{G}^* - \hat{\mathbf{G}}$, $\tilde{\boldsymbol{\xi}} = \boldsymbol{\xi}^* - \hat{\boldsymbol{\xi}}$, $\tilde{\boldsymbol{\eta}} = \boldsymbol{\eta}^* - \hat{\boldsymbol{\eta}}$, $\hat{\mathbf{G}}'_\xi = diag(g_{\xi l}) \in R^{L \times KL}$, $\hat{\mathbf{G}}'_\eta = diag\left(g_{\eta l}\right) \in R^{L \times L}$, $\mathbf{E} = \tilde{\mathbf{W}}^T \left(\hat{\mathbf{G}}'_\xi \tilde{\boldsymbol{\xi}} + \hat{\mathbf{G}}'_\eta \tilde{\boldsymbol{\eta}} \right) + \mathbf{W}^{*T} O \left(\mathbf{X}, \tilde{\boldsymbol{\xi}}, \tilde{\boldsymbol{\eta}} \right) + \boldsymbol{\varepsilon}(\mathbf{X})$, $O \left(\mathbf{X}, \tilde{\boldsymbol{\xi}}, \tilde{\boldsymbol{\eta}} \right)$ is the sum of the high-order arguments in the Taylor's series expansion. Based on the property of the RBF NN, it is assumed that $\|\mathbf{E}\| \leq \varphi(t)$, where $\varphi(t)$ is a nonnegative function.

The compensator of the dynamic adaptive RBF NN is designed as follows.

$$\mathbf{u}_{ns} = -\text{sgn}\left(\mathbf{B}^T \mathbf{P} \mathbf{e} \right) \hat{\varphi}(t) \tag{21}$$

where $\hat{\varphi}(t)$ is the estimation of $\varphi(t)$, $\mathbf{P}$ is the given symmetrical positive definite matrix and $\text{sgn}\left(\mathbf{B}^T \mathbf{P} \mathbf{e} \right)$ is the symbol matrix of $\mathbf{B}^T \mathbf{P} \mathbf{e}$.

Meanwhile, the dynamic adaptive RBF NN is adopted which can increase its hidden units on line from an original given number to an appropriate scalar with the approximation error growing until it is within the tolerable range. To avoid influence of the on-line topologic structure variability of the dynamic adaptive RBF NN on the real-time property of the system, the threshold logic unit (TLU) is designed to run in parallel with updating NN parameters, such as the weights, centres and widths. Note that this only

determines whether to add a new hidden unit rather than engaging in the feedback control loop directly. The input of the TLU is a sampling value of the current attitude error, and the sampling frequency is the same as the updating frequency of NN parameters. The output of the TLU determines whether it is necessary to add a new hidden unit according to the given growth criterion. Therefore, the TLU is defined as follows with two main components.

One is the operation rule, i.e., $\rho = \alpha \exp(e_{tra} - E_1) + (1-\alpha)\exp(e_{rms} - E_2)$, and the other is the growth criterion of hidden units formed by logical comparison:

$$\begin{cases} \rho > 1, & L = L + 1 \\ \rho \leq 1, & L = L \end{cases} \tag{22}$$

where L denotes the number of hidden units, $e_{tra} = \|\mathbf{e}(n)\|$ denotes the approximation error at sampling time n and $e_{rms} = \sqrt{\sum_{i=n-(M-1)}^{n} \|\mathbf{e}_i\|^2 / M}$ denotes the accumulative error covering a time sliding window M. E_1 and E_2 are the given bound values, and $0 < \alpha < 1$ is the influence factor. The parameters associated with the new hidden unit are given initially as $\xi_{L+1} = x(n)$ and $\eta_{L+1} = \lambda e_{tra}$, where λ is a regulatory factor.

Theorem 4.1. *For system (9), if there is a symmetrical positive definite matrix* $\mathbf{P}$ *that satisfies inequality (14), it can achieve closed-loop bounded stability under the control of the adaptive FTC (8). Assume that the number of hidden units in the dynamic adaptive RBF NN grows according to Equation (17) and its parameters (e.g., weight, centre and width) update by the following expressions:*

$$\dot{\hat{\boldsymbol{W}}} = \sigma_1 \hat{\mathbf{G}} \mathbf{e}^T \mathbf{P} \mathbf{B} \tag{23}$$

$$\dot{\hat{\boldsymbol{\xi}}} = \sigma_2 \left(\mathbf{e}^T \mathbf{P} \mathbf{B} \hat{\mathbf{W}}^T \hat{\mathbf{G}}'_{\xi} \right)^T \tag{24}$$

$$\dot{\hat{\boldsymbol{\eta}}} = \sigma_3 \left(\mathbf{e}^T \mathbf{P} \mathbf{B} \hat{\mathbf{W}}^T \hat{\boldsymbol{G}}'_{\eta} \right)^T \tag{25}$$

$$\dot{\hat{\boldsymbol{\varphi}}}_i = \sigma_4 \left\| \mathbf{e}^T \mathbf{P} \mathbf{B} \right\| \tag{26}$$

where σ_1, σ_2, σ_3, σ_4 *are all positive constants as the regulatory factors of the dynamic adaptive RBF NN.*

Proof: Consider the following Lyapunov candidate function:

$$V = \frac{1}{2}\mathbf{e}^T \mathbf{P} \mathbf{e} + \frac{1}{2\sigma_1} tr\left(\tilde{\mathbf{W}}^T \tilde{\mathbf{W}} \right) + \frac{1}{2\sigma_2} \tilde{\boldsymbol{\xi}}^T \tilde{\boldsymbol{\xi}} + \frac{1}{2\sigma_3} \tilde{\boldsymbol{\eta}}^T \tilde{\boldsymbol{\eta}} + \frac{1}{2\sigma_4} \tilde{\boldsymbol{\varphi}}^T \tilde{\boldsymbol{\varphi}}$$

where $\tilde{\boldsymbol{\varphi}} = \boldsymbol{\varphi} - \hat{\boldsymbol{\varphi}}$ is the compensation estimation error of the dynamic adaptive RBF NN. The above function is differentiated, which gives the following.

$$\dot{V} = \frac{1}{2}\dot{\mathbf{e}}^T \mathbf{P} \mathbf{e} + \frac{1}{2}\mathbf{e}^T \mathbf{P} \dot{\mathbf{e}} + \frac{1}{\sigma_1} tr\left(\tilde{\mathbf{W}}^T \dot{\tilde{\mathbf{W}}} \right) + \frac{1}{\sigma_2} \tilde{\boldsymbol{\xi}}^T \dot{\tilde{\boldsymbol{\xi}}} + \frac{1}{\sigma_3} \tilde{\boldsymbol{\eta}}^T \dot{\tilde{\boldsymbol{\eta}}} + \frac{1}{\sigma_4} \tilde{\boldsymbol{\varphi}}^T \dot{\tilde{\boldsymbol{\varphi}}}$$

According to $\dot{\tilde{\mathbf{W}}} = -\dot{\hat{\mathbf{W}}}$, $\dot{\tilde{\boldsymbol{\xi}}} = -\dot{\hat{\boldsymbol{\xi}}}$, $\dot{\tilde{\boldsymbol{\eta}}} = -\dot{\hat{\boldsymbol{\eta}}}$ and $\dot{\tilde{\boldsymbol{\varphi}}} = -\dot{\hat{\boldsymbol{\varphi}}}$, the following function can be derived by inserting Equations (20) and (23)-(26) as follows.

$$\begin{aligned} \dot{V} = \frac{1}{2}\mathbf{e}^T \left[(\mathbf{A} + \mathbf{B}\mathbf{K})^T \mathbf{P} + \mathbf{P}(\mathbf{A} + \mathbf{B}\mathbf{K}) \right] \mathbf{e} + \mathbf{e}^T \mathbf{P} \mathbf{B} \mathbf{E} \\ - \mathbf{e}^T \mathbf{P} \mathbf{B} \mathrm{sgn}\left(\mathbf{e}^T \mathbf{P} \mathbf{B} \right) \hat{\boldsymbol{\varphi}}(t) - \tilde{\boldsymbol{\varphi}}^T \left\| \mathbf{e}^T \mathbf{P} \mathbf{B} \right\| \end{aligned}$$

Thus, we obtain the following.

$$\begin{aligned}\dot{V} &\leq \frac{1}{2}\mathbf{e}^T\left[(\mathbf{A}+\mathbf{BK})^T\mathbf{P}+\mathbf{P}(\mathbf{A}+\mathbf{BK})\right]\mathbf{e}+\left\|\mathbf{e}^T\mathbf{PB}\right\|\|\mathbf{E}\| \\ &\quad -\left\|\mathbf{e}^T\mathbf{PB}\right\|\hat{\boldsymbol{\varphi}}(t)-(\boldsymbol{\varphi}-\hat{\boldsymbol{\varphi}})^T\left\|\mathbf{e}^T\mathbf{PB}\right\| \\ &\leq \frac{1}{2}\mathbf{e}^T\left[(\mathbf{A}+\mathbf{BK})^T\mathbf{P}+\mathbf{P}(\mathbf{A}+\mathbf{BK})\right]\mathbf{e}\end{aligned}$$

Based on the proof of Theorem 3.1, we derive that $\dot{V}<0$, and the system controlled by the adaptive FTC (8) can be a closed-loop bounded stable system. This completes the proof.

5. **Simulation and Comparison Results.** To verify the effectiveness of the proposed adptive FTC with control hedging (8), numerical simulation was performed for a certain 2U CubeSat.

5.1. **Parameters.** The useful parameters of the 2U CubeSat are given in Table 1, mainly including inertia moments used in Equation (2), and orbit altitude used to confirm mean value of local geomagnetic field matrix $\mathbf{B}(t)$. The initial attitude orientation is set to $\begin{bmatrix}\varphi & \theta & \psi\end{bmatrix}=\begin{bmatrix}1 & 2 & 1\end{bmatrix}^\circ$ with initial angle rate $\boldsymbol{\omega}=\begin{bmatrix}0.0001 & 0.0006 & -0.0003\end{bmatrix}$rad/s.

TABLE 1. Main satellite parameters

Mass (kg)	1.92
Inertia moments (kgm^2): Principal moments of inertia	$I_x=0.0115$, $I_y=0.0115$, $I_z=0.00369$
Products of inertia	Can be neglected
Orbit Altitude (km)	320
Attitude control type	Three axis control by three magnetorquers

Here, the external disturbance is considered as only the following gravitational torque. According to [17], it is defined as

$$\mathbf{T}_g=3.999\times10^{-6}\begin{bmatrix}(I_z-I_y)q_1\\(I_z-I_x)q_2\\0\end{bmatrix}$$

And also according to [17], we can obtain the following matrix.

$$\mathbf{B}_0=\begin{bmatrix}0 & 1.1407\times10^{-6} & -5.0828\times10^{-12}\\ -1.1407\times10^{-6} & 0 & 9.8757\times10^{-8}\\ 5.0828\times10^{-12} & -9.8757\times10^{-8} & 0\end{bmatrix}$$

As discussed in Section 4, the regulatory factors are chosen: $\gamma=1$, $L=3$, $\lambda=1$, $\alpha=0.6$, $\sigma_1=\sigma_2=\sigma_3=1$, $\sigma_4=0.8$.

In addition, we set $\mathbf{Q}=diag\begin{bmatrix}1.5 & 1.5 & 1.5 & 1.5 & 1.5 & 1.5 & 1.5\end{bmatrix}$. Thus, the feedback gain matrix $\mathbf{K}=\begin{bmatrix}0 & -0.47 & 0 & 0 & -2.01 & 0 & 0\\ 0 & 0 & -0.47 & 0 & 0 & -2.01 & 0\\ 0 & 0 & 0 & -0.47 & 0 & 0 & -2.01\end{bmatrix}$ is obtained according to Equations (15) and (16).

5.2. **Demonstration and results.** Assume that the magnetorquers in the roll, pitch and yaw axes each decrease by 30% of their normal values after 30000s.

The goal of this simulation is to verify stable performance of the CubeSat attitude control system with adaptive FTC with control hedging by comparing results obtained from adaptive FTC without hedging.

Figures 2 and 3 show the state responses obtained using adaptive FTC without and with control hedging, respectively. By comparing the simulation results of Figure 2(b) and Figure 3(b), it is clear that the attitude angle in the roll, pitch and yaw axes of the satellite in Figure 3(b) tend to stabilize more quickly and smoothly using the adaptive FTC with control hedging (8), which maintains angles within the desired range with only negligible error, although there is a tiny vibration at the time of fault occurrence. However, vibration does significantly influence stable attitude control, and the previous operation states are resumed. The control inputs can show the adjusting process distinctly. From Figure 2(d) and Figure 3(d), it is clear that control inputs vibrate at the time of beginning and faults occurring, but the degree of vibration in Figure 2(d) is more powerful than that in Figure 3(d); at the same time, the setting time of the former is slower than that of the latter. That is to say, the adaptive FTC with control hedging can achieve better control

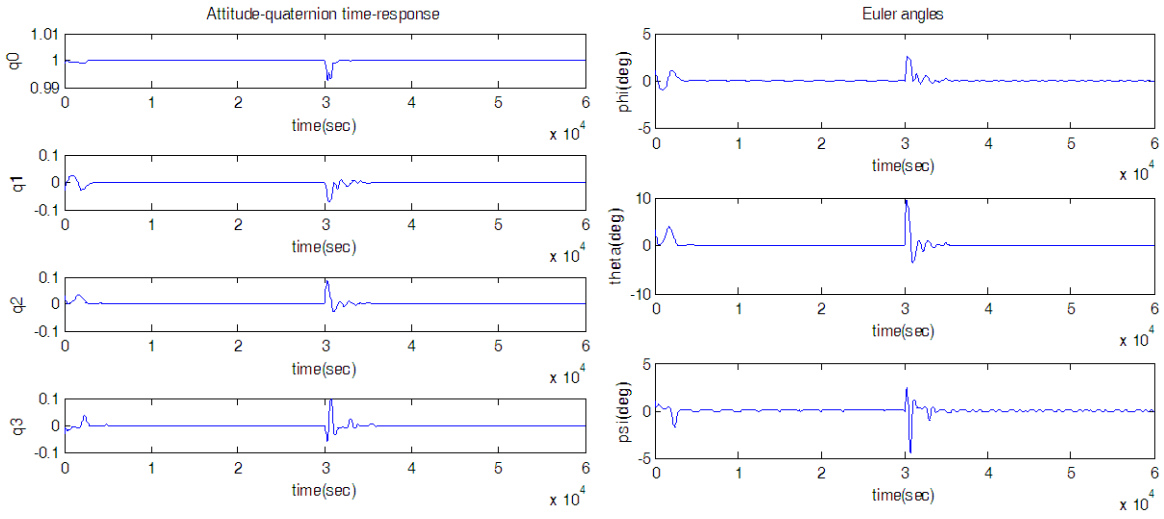

(a) Attitude-quaternion time-response

(b) Euler-angle time-response

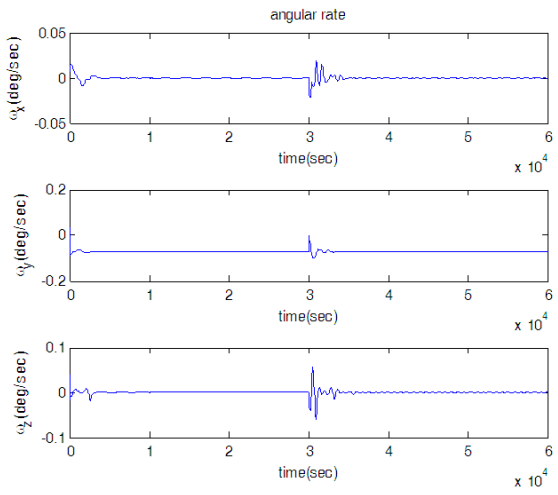

(c) Angular-rate time-response

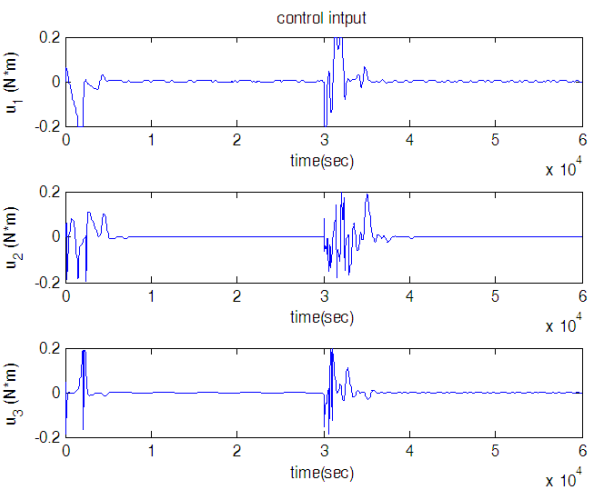

(d) Control-input time-response

FIGURE 2. Time responses under adaptive FTC without control hedging

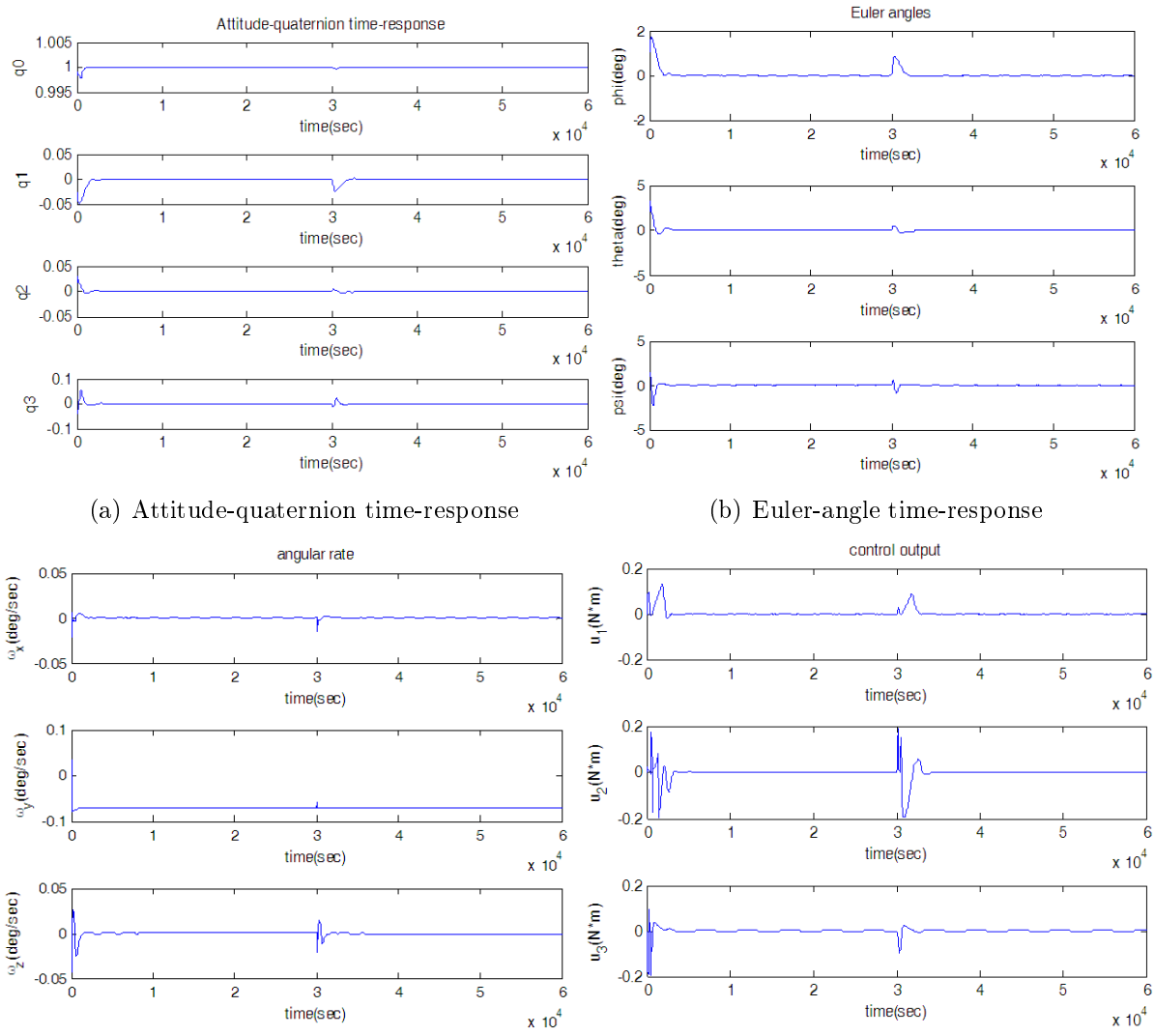

(a) Attitude-quaternion time-response

(b) Euler-angle time-response

(c) Angular-rate time-response

(d) Control-input time-response

FIGURE 3. Time responses under adaptive FTC with control hedging

capability than the adaptive FTC without control hedging. In view of these comparison results, the measure to add control hedging to the FTC can play an important role in improving dynamic control performance, especially when some faults occur which have the attitude abrupt varied. Also, Figures 2(a) and 2(c) and Figures 3(a) and 3(c) offer more complete demonstrations to verify the case that the proposed controller in the article can facilitate fault tolerant attitude control with high control performance.

6. **Conclusions.** The paper presents an adaptive attitude FTC with control hedging for CubeSats in LEO using 3-axis magnetorquers as its attitude control actuators. This control scheme uses H-infinity robust control with control hedging to deal with uncertain external disturbances and input saturation, and adopts the dynamic adaptive RBF NN to eliminate the unknown dynamics caused by actuators faults. It can be a reliable method in the sense that closed-loop bounded stability for attitude control system was guaranteed. Numerical simulations are carried out to verify the effectiveness of the presented FTC scheme by using a 2U CubeSat of QB50 project in ACSER UNSW as the plant. By comparing the results of the adaptive FTC with control hedging and those without control hedging, it is shown that the control performance of the former method is better than

that of the latter, such as convergence rate, overshoot, and settling time. It is necessary to point out that, in this paper, we just investigate the case of partial loss of actuators effectiveness rather than any other faults which will be studied as some of our future work.

Acknowledgment. This work is supported by the National Natural Science Foundation of China (61573189, 61403207), and the Jiangsu Natural Science Foundation of Jiangsu Province (BK20140045). The authors also gratefully acknowledge the helpful comments and suggestions of the reviewers, which have improved the presentation.

REFERENCES

[1] A. M. Oluwatosin, Y. Hamam and K. Djouani, Attitude control of a CubeSat in a circular orbit using magnetic actuators, *Africon*, pp.1-9, 2013.
[2] J. Li, M. Post, T. Wright et al., Design of attitude control for CubeSat-class NanoSatellite, *Journal of Control Science and Engineering*, vol.2013, 2013.
[3] A. Ali, M. R. Mughal, H. Ali et al., Innovative power management, attitude determination and control tile for CubeSat standard NanoSatellites, *Acta Astronautica*, vol.96, pp.116-127, 2014.
[4] M. A. Post, J. Li and R. Lee, Design and construction of a magnetic field simulator for CubeSat attitude control testing, *Journal of Instrumentation, Automation and Systems*, vol.1, no.1, pp.1-9, 2014.
[5] S. Spangelo and B. Longmier, Optimization of CubeSat system-level design and propulsion systems for Earth-Escape missions, *Journal of Spacecraft & Rockets*, pp.1-12, 2015.
[6] A. R. Walker and K. Cohen, Fuzzy logic attitude control of a magnetically actuated CubeSat, *Aerospace Materials*, Aerospace Engineering, University of Cincinnati, 2013.
[7] W. C. Luo, Y. C. Chu and K. V. Ling, H-infinity inverse optimal attitude-tracking control of rigid spacecraft, *Journal of Guidance, Control, and Dynamics*, vol.28, pp.481-493, 2005.
[8] R. Kristiansen, P. J. Nicklasson and J. T. Gravdahl, Satellite attitude control by quaternion-based backstepping, *IEEE Trans. Control Systems Technology*, vol.17, no.1, pp.227-232, 2009.
[9] H. Yoon and B. N. Agrawal, Adaptive control of uncertain Hamiltonian multi-input multi-output systems: With application to spacecraft control, *IEEE Trans. Control Systems Technology*, vol.17, no.4, pp.900-906, 2009.
[10] Y. M. Zhang and J. Jiang, Bibliographical review on reconfigurable fault-tolerant control systems, *Annual Reviews in Control*, vol.32, no.2, pp.229-252, 2008.
[11] M. Saif, B. Ebrahimi and M. Vali, Fault tolerant control of satellite formation flying using second order sliding mode control, *IEEE International Conference on Systems, Man, and Cybernetics*, Anchorage, AK, 2011.
[12] Godard and K. D. Kumar, Fault tolerant reconfigurable satellite formations using adaptive variable structure techniques, *Journal of Guidance, Control, and Dynamics*, vol.33, no.3, pp.969-983, 2010.
[13] A. Zou and K. D. Kumar, Adaptive fuzzy fault-tolerant attitude control of spacecraft, *Control Engineering Practice*, vol.19, no.1, pp.10-21, 2011.
[14] H. Lee and Y. Kim, Fault-tolerant control scheme for satellite attitude control system, *IET Control Theory and Applications*, vol.4, no.8, pp.1436-1450, 2010.
[15] B. Xiao, Q. Hu and Y. Zhang, Adaptive sliding mode fault tolerant attitude tracking control for flexible spacecraft under actuator saturation, *IEEE Trans. Control Systems Technology*, vol.20, no.6, pp.1605-1610, 2012.
[16] W. C. Cai, X. H. Liao and Y. D. Song, Indirect robust adaptive fault-tolerant control for attitude tracking of spacecraft, *Journal of Guidance, Control, and Dynamics*, vol.31, no.5, pp.1456-1463, 2008.
[17] F. S. Holberg, Optimal attitude control of a double cubesat using magnetorquers, *Project Report*, Department of Engineering Cybernetics, NTNU, 2011.
[18] Y. Liu and S. Hu, Fuzzy H-infinity robust feedback control for uncertain nonlinear system with time-delay based on fuzzy model, *Control Theory & Applications*, vol.20, no.4, pp.497-502, 2003.
[19] M. Zhang and S. Hu, Dynamic adaptive neural network control of systems with uncertain multiple-time-delays, *Systems Engineering and Electronics*, vol.31, no.2, pp.434-438, 2009.
[20] J. D. Boskovic, S. M. Li and R. K. Mehra, Robust tracking control design for spacecraft under control input saturation, *Journal of Guidance, Control, and Dynamics*, vol.27, no.4, pp.627-633, 2004.

[21] P. Tsiotras and J. Luo, Control of underactuated spacecraft with bounded inputs, *Automatica*, vol.36, no.8, pp.1153-1169, 2000.

[22] T. Gubner, M. Jost and J. Adamy, Controller design for a class of nonlinear systems with input saturation using convex optimization, *Systems & Control Letters*, vol.61, pp.258-265, 2012.

[23] L. Qiao, M. Zhang, B. Osborne and A. Dempster, Attitude determination and control system (ADCS) of UNSW QB50 project "UNSW EC0", *Australian Space Science Conference*, Sydney, Australia, 2013.

[24] H. Lee and Y. Kim, Fault-tolerant control scheme for satellite attitude control system, *IET Control Theory and Applications*, vol.4, no.8, pp.1436-1450, 2010.

[25] Y. Li, N. Sundararajan and P. Saratchandran, Neuro-controller design for nonlinear fighter aircraft maneuver using fully tuned RBF networks, *Automatica*, vol.37, pp.1293-1301, 2001.

[26] Y. Lu, N. Sundararajan and P. Saratchandran, Performance evaluation of a sequential minimal RBF neural network learning algorithm, *IEEE Trans. Neural Network*, vol.9, no.2, pp.308-318, 1998.